

Optical Interferometers

As we already started to unveil last week, interferometry is an extremely powerful toolset for engineering and modern physics. In the next three weeks you will see how the same tools and concepts have been used for over a century to support fundamental and theoretical research - from the foundations of electromagnetism to general relativity - as well as support some of the most sensible and robust state-of-the-art optical sensors - from very precise accelerometers to robust magnetic field sensing. Besides, we will try to capture the advantages and disadvantages of various designs and their potential applications, while also studying the challenges involved in detection and ways to circumvent them, from classical to quantum theory.

The essence of interferometry resides in the precise measurement of the phase difference between waves as they combine. Such phase differences occur due to variations on characteristic length scales below light wavelength, acting like a **microscopic ruler** and thus offering humans a window into the mesoscopic realm.

For this fifth week, we delve into three well-known designs of interferometers - **Michelson**, **Mach-Zehnder**, and **Sagnac** interferometers - exploring their historical framing, mathematical framework, and some applications. Then, connecting to the common language we established for the sensors and through some hands-on activities (experimental and computational), we will explore the potential of interferometry for optical sensing.

But before entering on the description of the interferometers themselves, let us introduce a handy matrix formalism to deal with interferometers when these involve beam splitters and other optical elements.

1 Transfer Matrix Formalism

While it is easy to explain wave interference with just two waves, analyzing optical systems involving components such as beam splitters and forward and backward propagating waves traveling the same paths can become rather complicated if one wants to keep all the mathematical details. In this case, the transfer matrix formalism comes as a very handy tool, simplifying the approach. In short, assuming a 50:50 beam splitter and the ports nomenclature of Figure 48, we have the resulting fields⁴³

Week

V

Section 2. Michelson Interferometer

Section 3. Mach-Zehnder Interferometer

Section 4. Sagnac Interferometer

Table 4. Contents for WEEK V

⁴³ we assume the Loudon symmetric beam splitter

$$\begin{aligned} \begin{bmatrix} \mathbf{E}_3 \\ \mathbf{E}_4 \end{bmatrix} &= \frac{1}{\sqrt{2}} \begin{bmatrix} 1 & i \\ i & 1 \end{bmatrix} \begin{bmatrix} \mathbf{E}_1 \\ \mathbf{E}_2 \end{bmatrix} \\ &= \overline{\mathbf{PS}} \begin{bmatrix} \mathbf{E}_1 \\ \mathbf{E}_2 \end{bmatrix} \end{aligned} \quad (1.1)$$

In similar manner, one case use a matrix of the form

$$\overline{\mathbf{PS}} = \begin{bmatrix} e^{i\Delta\phi} & 0 \\ 0 & 1 \end{bmatrix} \quad (1.2)$$

to account for a phase shift $\Delta\phi$ in one of the paths. For example, the propagation over a distance L may be taken into account as a phase term kL (or $-kL$ for $+\omega$ convention). Furthermore, this phase shift may also be a spatial distribution of phase in the transverse directions, say $\Delta\phi(x, y)$. Finally, a mirror can be taken into account as a phase shift term, usually of π .

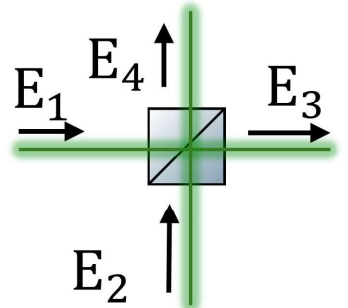


Figure 48. Beamsplitter port nomenclature for the transfer matrix formalism.

2 Michelson Interferometer

Born in 1852, Albert Michelson is one of the fathers of the North American Physics community, being the first one to be awarded the Nobel Prize in 1907 "for his optical precision instruments and the spectroscopic and metrological investigations carried out with their aid".

But interestingly, the success of Michelson was mostly a product of his drive to probe a wrong hypothesis⁴⁴: the presence of the luminiferous aether, a medium utilized for light waves to propagate through space. Indeed, Michelson designed an ultraprecise interferometer - **Michelson Interferometer** - and mounted their apparatus on a large stone block floating in a pool of mercury to isolate vibrations and to allow easy rotation of the experiment⁴⁵. At that time, aether was thought to be a fixed, invisible medium filling all space, and as Earth was believed to move through this aether, Michelson and Morley were expecting a variation of the signal of the interferometer depending on the orientation of the experiment. With unbeatable precision for that time, the negative outcome of the Michelson-Morley experiment(1887) was strong evidence of the inexistence of aether. Despite the "failure" to detect aether⁴⁶, the Michelson interferometer became an essential tool in the scientific community due to its unparalleled precision. The design of the Michelson interferometer (Figure 49) starts with a coherent light source, such as a laser, that emits a beam steered towards a beamsplitter. This beamsplitter (say 50:50) divides the incoming light into two paths - call it reference path 4 and measurement path 3. The light is then reflected by a mirror in each path and recombined at the beamsplitter. For the present case, we consider that

⁴⁴ "The only real mistake is the one from which we learn nothing"

⁴⁵ a very rudimentary optical table

⁴⁶ and which apparently contradicted the Fizeau moving media experiment, a discrepancy solved later by Einstein's special relativity

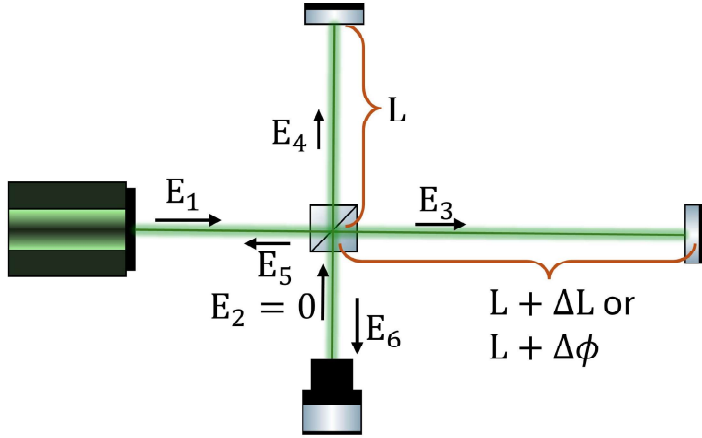


Figure 49. Configuration of the Michelson Interferometer.

there is an additional path length of t in the measurement arm, which going back and forth amounts to a total of path length $2\Delta L$, and corresponding phase shift $2\Delta\phi = 2k\Delta L$. Assuming that the polarization stays the same, it is easy to get under the transfer matrix formalism (discarding the effect of the mirrors and the phase term of propagation along the same path)

$$\begin{bmatrix} \mathbf{E}_5 \\ \mathbf{E}_6 \end{bmatrix} = \overline{BS} \cdot \overline{PS} \cdot \overline{PS} \cdot \overline{BS} \begin{bmatrix} \mathbf{E}_1 \\ \mathbf{E}_2 \end{bmatrix} \\ = \frac{1}{2} \begin{bmatrix} 1 & i \\ i & 1 \end{bmatrix} \begin{bmatrix} e^{i\Delta\phi} & 0 \\ 0 & 1 \end{bmatrix} \begin{bmatrix} e^{i\Delta\phi} & 0 \\ 0 & 1 \end{bmatrix} \begin{bmatrix} 1 & i \\ i & 1 \end{bmatrix} \begin{bmatrix} \mathbf{E}_1 \\ \mathbf{E}_2 \end{bmatrix}. \quad (2.1)$$

For the simple case of input state only in one port, i.e. $\mathbf{E}_2 = 0$, it is straightforward to get

$$\begin{bmatrix} \mathbf{E}_5 \\ \mathbf{E}_6 \end{bmatrix} = \frac{1}{2} \begin{bmatrix} (e^{2i\Delta\phi} - 1) \mathbf{E}_1 \\ i(e^{2i\Delta\phi} + 1) \mathbf{E}_1 \end{bmatrix}. \quad (2.2)$$

which taking the intensities at each port gives

$$\begin{aligned} I_5 &= \frac{I_1}{2}(1 - \cos(2\Delta\phi)) = \frac{I_1}{2}(1 - \cos\left(\frac{4\pi\Delta L}{\lambda}\right)) \\ I_6 &= \frac{I_1}{2}(1 + \cos(2\Delta\phi)) = \frac{I_1}{2}(1 + \cos\left(\frac{4\pi\Delta L}{\lambda}\right)). \end{aligned} \quad (2.3)$$

It is thus trivial to observe that if $\Delta L = 0$ there will be constructive interference at port 6 and destructive interference at path 5. Besides, the signal recorded at 6 will be sensitive to variations of ΔL and therefore may be suitable for multiple sensing applications. This way, the Michelson interferometer has a plethora of applications ranging from fundamental science to

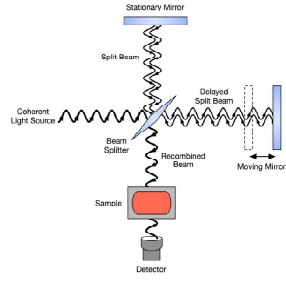
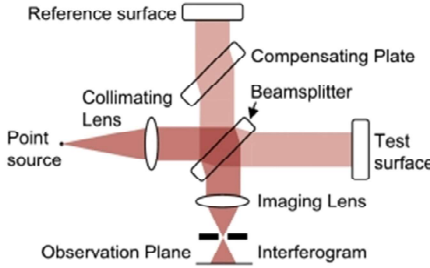


Figure 50. Applications of the Michelson interferometer: LIGO, Twyman-Green, and FTIR.

practical technology. Notable applications include precise metrology such as gravitational wave detection in LIGO, but also optical components testing (under the Twyman-Green configuration) and spectroscopy (being one of the working principles of Fourier Transform Infrared (FTIR) spectroscopy).

3 Mach-Zehnder Interferometer

With a similar working principle to the Twyman-Green configuration, the Mach-Zehnder interferometer (1891) also uses of an expanded beam of collimated light but simplifies the interpretation of the observed fringes by passing light through the sample only once. Another advantage is the access to an additional port, which comes in phase opposition to the other and may be utilized for noise mitigation strategies or to enable other types of signal analysis and interrogation as we will explore next week.

The Mach-Zehnder interferometer utilizes two beam splitters together with two mirrors to divide the beam into 2 paths before recombining the beams. Following the configuration of Figure 51, we get a very similar formula to that obtained for the Michelson interferometer,

$$\begin{aligned} I_5 &= \frac{I_1}{2}(1 - \cos(\Delta\phi)) \\ I_6 &= \frac{I_1}{2}(1 + \cos(\Delta\phi)) \end{aligned} \quad (3.1)$$

and thus the signal at the output ports of the beam splitter will be sensitive to any phase variation induced in the measurement arm 3.

A very common way to use the Mach-Zehnder is to add a small displacement on the lateral separation of both beams, together with a small angle that can be controlled by the reference mirror (see Figure 52). If needed, one can also expand the reference arm. Considering a small angle θ in the $x0z$ plane,

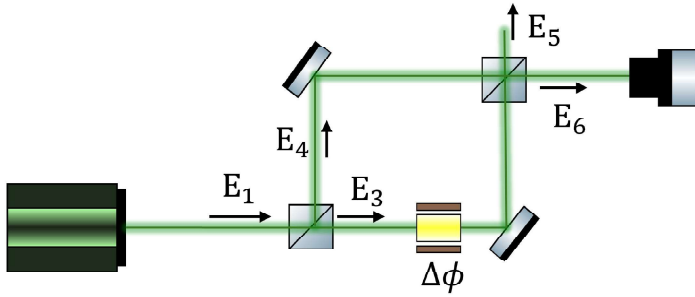


Figure 51. Configuration of the Mach-Zehnder Interferometer.

this will lead to a phase difference on the reference path $\Delta\phi_{ref} = (k \sin \theta)x$

$$\begin{aligned} I_5 &= \frac{I_1}{2} [1 - \cos(\Delta\phi + (k \sin \theta)x)] \\ I_6 &= \frac{I_1}{2} [1 + \cos(\Delta\phi + (k \sin \theta)x)] \end{aligned} \quad (3.2)$$

This way, a fringe pattern varying across the transverse plane may be generated (see Figure 52), which can be used to observe wavefront deformations and relate with sample properties (e.g. spatial distribution of the refractive index).

The versatility of the Mach-Zehnder Interferometer has led to its widespread use across various fields, including metrology for gas flows and plasmas, and biological imaging (e.g. Optical coherence tomography). In addition, Mach-Zehnder is also widely utilized as a modulator for telecommunication purposes, utilizing phase shifts in one arm to generate amplitude modulation at the output ports. Finally, the Mach-Zehnder also played a crucial role in foundational experiments in quantum mechanics, including tests of quantum entanglement and the principle of superposition, as we will later explore in this curricular unit.

3.1 Digital Off-Axis Holography

Digital off-axis holography concerns a technique of using interference and digital signal processing to reconstruct the complex electric field and thus access the spatial phase distribution on the measurement arm. In particular, the Mach-Zehnder interferometer serves as an excellent platform for implementing digital off-axis holography due to the possibility of controlling fringe spacing and shape.

Unlike traditional in-line holography, off-axis holography utilizes a deliberate angle between the object and reference beams as they are recombined. This angle separation (that controls fringe spacing and shape) ensures the spatial separation of the hologram zeroth-order and conjugate images in the

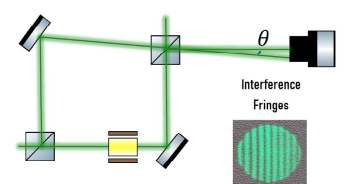


Figure 52. Adding an angle between the beams for the interference fringes.

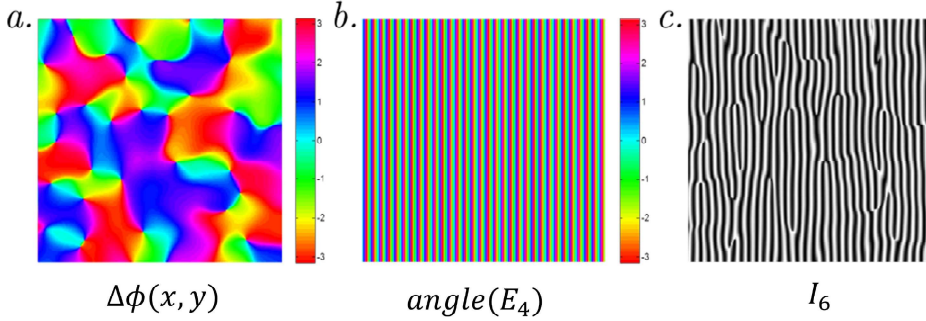


Figure 53. Filtering Process of the Digital Off-Axis holography.

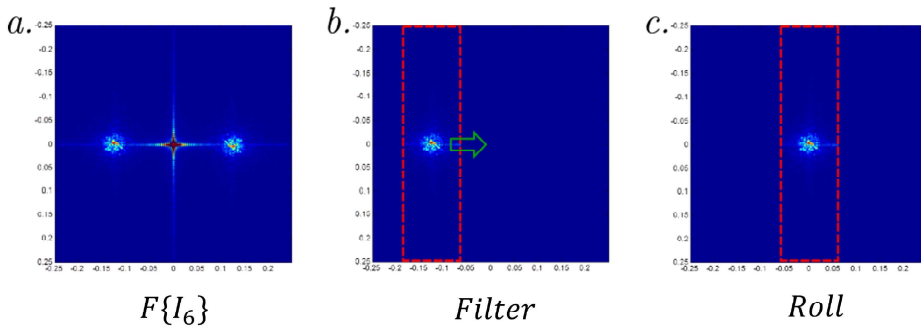


Figure 54. Filtering Process of the Digital Off-Axis holography.

frequency domain, facilitating easier and more efficient hologram reconstruction. Considering the spatial phase distribution we want to measure in path 3 to be described by $\Delta\phi(x, y)$ you can recover the previously derived formula for the path 6 and generalize it for the following assumptions:

- Distinct intensities $I_3(x, y)$ and $I_4 = \text{const.}$;
- Reference and measurement wavevectors define two angles θ_1 and θ_2 in the $x0z$ and $y0z$ planes, for which we also define $k_x = k \sin \theta_1$ and $k_y = k \cos \theta_2$.

The signal at port 6 becomes then

$$I_6 = I_3(x, y) + I_4 + \sqrt{I_3(x, y)I_4} \cos(\Delta\phi + k_x x + k_y y). \quad (3.3)$$

The holographic image - i.e. the complex field $E_3 = \sqrt{I_3}e^{i\Delta\phi(x,y)}$ - can then be reconstructed by digital signal processing in the following manner:

- First, blocking the reference path, you record with a camera the profile $I_3(x, y)$;
- Secondly, with the reference path on, you record with a camera the interferogram profile $I_6(x, y)$;

- Transforming I_6 to Fourier domain using a numerical 2D FFT, you will encounter:
 - A spot close to the center $(k_x, k_y) = 0$ corresponding to the zeroth order and to the Fourier transform of the intensity $F\{I_3 + I_4\}$;
 - Two spots localized in two of the quadrants: one will correspond to the term $E_3 E_4^*$ (i.e. centered in $(-k_x, -k_y)$ in the Fourier domain, denominated -1 order) whereas the other will correspond to $E_3^* E_4$ (i.e. centered in (k_x, k_y) in the Fourier domain, denote +1 order);
- Localize the -1 order point and optimize the tilt of the mirror to control the center point in order to prevent overlap of order 0 and order -1;
- Apply a filter in the Fourier domain, keeping only the terms related to that order - for example applying a circular window - which leaves you with the term $F\{\sqrt{I_3 I_4} e^{\Delta\phi(x,y) - i(k_x x + k_y y)}\}$;
- Choosing the correct center point, execute a roll necessary to recenter the transform at the origin, giving you $F\{\sqrt{I_3 I_4} e^{\Delta\phi(x,y) - i(k_x x + k_y y)} e^{+i(k_x x + k_y y)}\}$, where the second term is added due to the shift in the Fourier domain and Fourier transform properties;
- Apply the inverse 2D Fourier transform to obtain the complex field, $F^{-1}\{F\{\sqrt{I_3 I_4} e^{\Delta\phi(x,y)}\}\} = \sqrt{I_3 I_4} e^{\Delta\phi(x,y)}$;

This technique allows measuring the complex field with just a single shot and is widely used in advanced imaging solutions. For example, it has found applications in biological imaging, microfluidics, and materials science, where detailed three-dimensional reconstructions and precise measurements of optical path length changes are invaluable. Another common application is imaging through complex media, where it enables one to see through diffusive media or multimode fibers, for example.

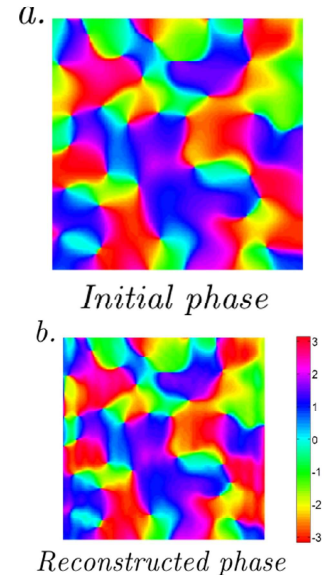


Figure 55. Result of the Off-axis holography.

4 Sagnac Interferometer

Another interesting interferometer design is the Sagnac interferometer, developed by French physicist Georges Sagnac in 1913. As the Michelson interferometer, this instrument was also designed to probe the existence of the luminiferous aether. Aether was not found but instead, it was discovered a rotation-induced phase shift of light, a phenomenon now known as the Sagnac effect.

In the Sagnac interferometer, as shown in Figure 56, the two beams traverse the same closed path in opposite directions. Its unique configuration allows to detect phase shifts caused by non-reciprocal effects⁴⁷ such as rotational motion. The closed path feature also offers several advantages:

- **Easier to align:** utilizing the same path makes it very easy to align;
- **Robustness to External Vibrations:** featuring symmetry in both arms, it is less susceptible to external vibrations and thermal fluctuations;
- **Simplicity and Versatility:** involves just a few components and does not require special care about the coherence length of the laser.

Not surprisingly the mathematical formulation is the same as the last two examples. Regarding the phase difference, we will consider the simplified case of the ring interferometer⁴⁸. Considering the rotation motion of angular velocity ω we will have that the time taken by field E_3 to travel the distance of the interferometer is

$$t_3 = \frac{2\pi R + \Delta L}{c} = \frac{2\pi R + R\omega t_3}{c} \quad (4.1)$$

where $\Delta L = R\omega t_3$. Conversely, field E_4 will travel less distance, leading to

$$t_4 = \frac{2\pi R - R\omega t_4}{c}. \quad (4.2)$$

The total time difference becomes

$$\Delta t = t_3 - t_4 = \frac{4\pi R^2 \omega}{c^2 - R^2 \omega^2} \quad (4.3)$$

which for $R\omega = v \ll c$ translates into a phase difference

$$\Delta\phi = \frac{2\pi c \Delta t}{\lambda} = \frac{8\pi A \omega}{\lambda c} \quad (4.4)$$

where A stands for the area enclosed by the light path, λ the wavelength of the light, and c the speed of light vacuum.

In the particular case of the Sagnac interferometer, a fiber-optic configuration is particularly interesting as it allows for a significant increase in the effective path length by utilizing a coiled version, multiplying the phase length by a factor of N with N being the number of fiber optic coils utilized.

Such ultra-high sensitivity combined with the robustness and compactness of the system, enable one of the most successful applications of the Sagnac interferometer as an optical sensor: the high-precision fiber optic gyroscopes. In

⁴⁷ i.e. distinct effects for the distinct directions

⁴⁸ although a general formulation can be achieved under relativistic theory and infinitesimal path arguments

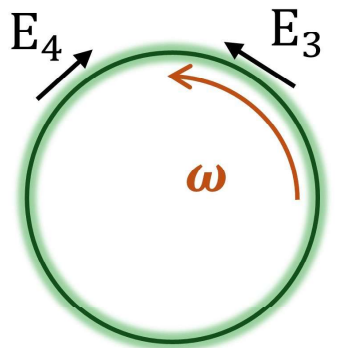


Figure 56. Sagnac configuration.

addition, such gyroscopes also feature immunity to electromagnetic interference, making them ideal for use in harsh environments or critical applications environments such as satellites, submarines, and autonomous vehicles.

Week

VI

5 Fabry-Perot Interferometer

So far, we have explored interferometric configurations involving a simple two-wave interference process. However, besides the possible mathematical challenge that may come with it, there is no limitation on extending the interferometer principle to a situation with more than two waves. The Fabry-Perot Interferometer (FPI) is an example of a device in the field of optical sensing that exploits the principles of multiple wave interference to measure, amongst others, the spectral properties of light. Its design consists fundamentally of two parallel, highly reflective mirrors, creating a resonant cavity that enhances certain wavelengths of light through constructive interference.

Our starting point is the analysis of the combination of multiple wave reflections occurring on a thin dielectric film. Looking at Figure 57, our intuition on wave interference leads us to think that the light waves reflecting back and forth between the boundaries of the dielectric layer may result in a resonant cavity. For the sake of simplicity, we will consider that we have the effective reflection and transmission coefficients t_0 , t'_0 , and r_1 , which, depending on the polarization, can change according to Fresnel equations.

Looking at the first transmitted wave, we have

$$E_{t_0} = E_0 t_0 t'_0. \quad (5.1)$$

It is easy to generalize the N-th transmitted wave

$$E_{t_N} = E_0 r^{2N} t_0 t'_0 e^{iN\delta} \quad (5.2)$$

with

$$\delta = \frac{4\pi n d \cos(\theta)}{\lambda} \quad (5.3)$$

with n the refractive index inside, meaning that the total transmitted field will be given by a geometric series

$$E_t = E_0 \sum_{n=0}^{\infty} r^{2N} t_0 t'_0 e^{iN\delta} = E_0 t_0 t'_0 \frac{1}{1 - r^2 e^{i\delta}}. \quad (5.4)$$

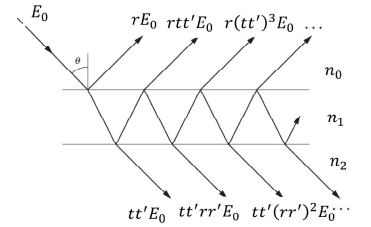


Figure 57. Multiple reflections and total transmitted intensity.

The most usual case is unpolarized light.

The transmitted intensity can be derived from the electric field as

$$I_t = I_0 T^2 \frac{1}{1 + R^2 - 2R \cos(\delta)} \quad (5.5)$$

where we consider $T = |t_0|^2 = |t'_0|^2$ and $R = |r|^2$. Using the definition of coefficient of finesse $F = 4R/(1 - R^2)$ it can be further simplified to

$$I_t = I_0 T^2 \frac{1}{1 + F \sin^2(\delta/2)}. \quad (5.6)$$

By plotting the transmitted intensity over the total intensity as a function of the phase difference, it is easy to understand what happens in a Fabry-Perot interferometer and the actual role of the finesse coefficient. By analyzing Figure 58, it is possible to see that a higher finesse coefficient relates to higher visibility, whereas a lower finesse coefficient leads to lower (almost sinusoidal-like) visibility.

Recovering the phase difference formula, it is possible to demonstrate that the maximum will occur at

$$\delta/2 = m\pi \rightarrow \cos(\theta) = \frac{m\lambda}{2nd} \quad (5.7)$$

meaning that:

- For normal incidence $\theta = 0$, the FPI is sensitive to variations of thickness, wavelength, and index of refraction;
- With a lens at the output (incident angles are transformed into distances in the plane), you will obtain different peaks depending on the wavelength of your source.

Motivated by the last observation we can also explore what happens in an FPI as a function of the wavelength (see Figure 58). In this case, two figures of merit can be helpful to describe the experimental settings and the characteristics of a sensor: the free spectral range and the Finesse.

Free Spectral Range: The Free Spectral Range (FSR) corresponds to the separation in frequency between successive transmission peaks. In frequency it is given by:

$$FSR_f = \frac{c}{2n_1 d \cos(\theta)} \quad (5.8)$$

where c is the speed of light, and d is the mirror separation. In wavelength, using $f = c/\lambda$ which leads to $df = -c/\lambda^2 d\lambda$ this can be expressed

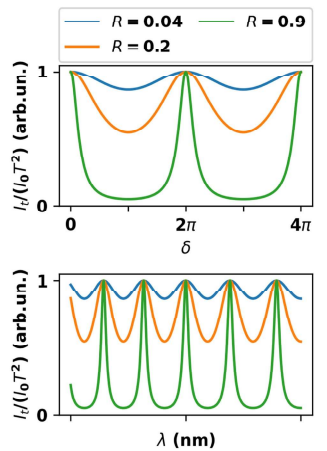


Figure 58. Transmitted intensity in function of path distance and wavelength.

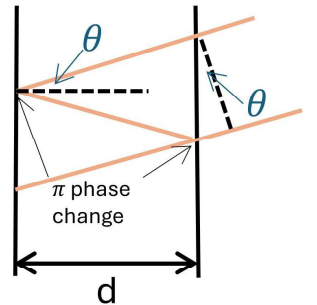


Figure 59. Path distance.

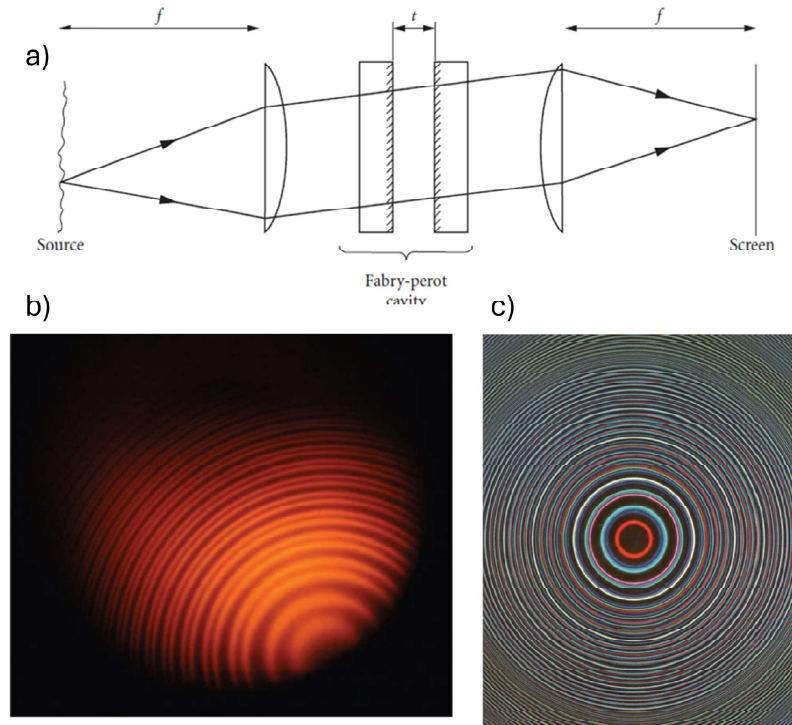


Figure 60. Spectrometry using a Fabry-Perot. Different wavelengths will have distinct resonance angles, ultimately leading to circle structures when passing the setup (a). (b) Sodium lamp doublet and (b) white light spectrum.

as

$$FSR_\lambda = \frac{\lambda_0^2}{2n_1 d \cos(\theta)} \quad (5.9)$$

Finesse: The finesse \mathcal{F} (not to be confounded with the coefficient of finesse) measures the spectral resolution of the Fabry-Perot and is defined as the ratio of the FSR to the full width at half maximum (FWHM) of the transmission peaks:

$$\mathcal{F} = \frac{FSR}{FWHM} = \frac{\pi}{2\arcsin(1/F)} \approx \frac{\pi\sqrt{F}}{2} \quad (5.10)$$

where the last approximation is valid for high-reflective mirrors $R \approx 1$.

Overall, Fabry-Perot interferometers offer several distinct advantages that make them particularly valuable for optical sensing applications:

- **Versatility, compactness, and simplicity of design:** FPIs operate from UV to IR wavelength ranges, needing only a few optical components and can be deployed either in free space or fiber configurations;
- **Sensitivity and High Spectral Resolution:** FPIs are highly sensi-

tive to changes in wavelength, thus useful to monitor spectral changes (e.g. environmental monitoring applications);

- **Tunability and Multiplexing capabilities:** The resonant cavity of an FPI can be easily tuned by adjusting the distance between the mirrors, which changes the resonance conditions of the cavity. This tunability allows for selective filtering and analysis of specific wavelengths.
- **Stability and Reliability:** FPIs are known for their stability and reliability over time and can be easily integrated with other optical elements and electronic detection systems.

Finally, in terms of applications, Fabry-Perot interferometers are a popular choice for wavelength-related or wavelength-based analysis, from **environmental monitoring** to **fiber-based microphones**, and from **telecommunications** to **laser spectrometry** (i.e. measuring the spectrum of a laser).

6 Concluding Remarks

Throughout this chapter, we have seen how different interferometric designs present opportunities and unique advantages for sensing applications that span a wide range of scientific and technological fields. Although we covered the most common ones - **Michelson**, **Mach-Zehnder**, Sagnac, and **Fabry-Perot** interferometers - there many other configurations (see Figure ?? for classical and historical examples). Yet, the same principles you learned in this chapter hold in every other configuration, meaning that in the classical picture, you have all the tools that you need to analyze any configuration, from free space to fiber-based and even integrated optics.

To conclude, interferometers translate variations in the environment into phase differences that ultimately lead to variations in the intensity measured at the output. Now, it is time to discuss how to measure this intensity.

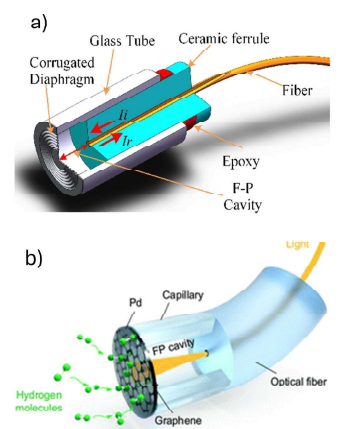


Figure 61. Example applications of the Fabry-Perot interferometer in Fiber Sensing solutions for (a) a microphone and (b) biochemical sensing.

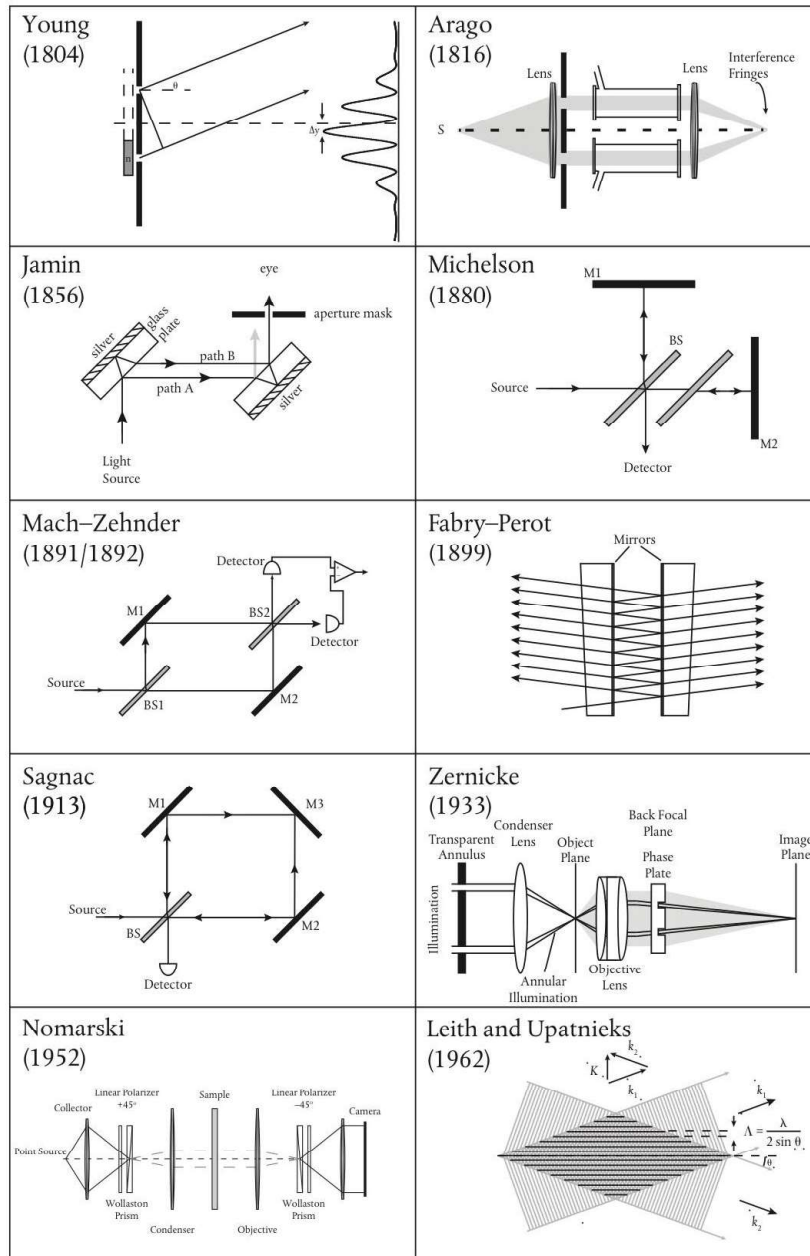


Figure 62. Multiple configurations of interferometers over the last two centuries.